224 RAPID-SCAN DUAL-POLARIZATION WSR-88D OBSERVATIONS OF OKLAHOMA HAILSTORMS ON 26 MARCH 2017

ARTHUR WITT*
NOAA/National Severe Storms Laboratory, Norman, OK

CHARLES M. KUSTER
CIMMS/Univ. of Oklahoma, Norman, OK

1. INTRODUCTION

During the afternoon and evening of 26 March 2017, two supercell hailstorms occurred within 100 km of three WSR-88Ds (KOUN, KCRI and KTLX) in central Oklahoma. There were 15 reports of large hail from the two storms, ranging from 25–83 mm in diameter. One of the radars (KOUN) collected rapidly-updating 90° sector scans of the two storms, with volume update times $<$ 2 min. The other radars (KCRI and KTLX) collected full 360° elevation scans, with volume update times of 6–7 min. The study presented here examines and compares the radar observations of the two storms from the three WSR-88Ds to determine the benefits of shorter volume update times and the extent of variations between the three radars for several storm intensity and dual-polarization parameters.

2. DATA AND METHODS

a. Hailstone observations

The first hailstorm, referred to as the Paoli hailstorm (PH), was examined from 2100 UTC to 0100 UTC (hereafter all times are in UTC). At 2100, the PH was located ∼200° and 109 km from KOUN. Over the next 4 hours, it moved northeastward at ∼14 m s^{-1} (Fig. 1), and at 0100 was located ∼84° and 120 km from KOUN. During this 4 hour period, seven reports of large hail were recorded for the PH (in the severe weather reports log of the Storm Prediction Center), ranging from 25–64 mm in diameter (Table 1).

The second hailstorm, referred to as the Ada hailstorm (AH), was examined from 2131 to 0100. At 2131, the AH was located ∼187° and 119 km from KOUN. Over the next 3.5 hours, it moved northeastward at ∼11 m s^{-1}, and at 0100 was located ∼112° and 112 km from KOUN. During this 3.5 hour period, eight reports of large hail were recorded for the AH, ranging from 25–83 mm in diameter (Table 2).

b. Radar-based parameters

Storm intensity was assessed via three radar parameters. The two velocity-based parameters were derived from the radial velocity data, with the reflectivity-based parameter determined after "mapping" the radial reflectivity data to a 3D latitude-longitude-height grid at a resolution of 0.01° x 0.01° x 1.0 km (Lakshmanan et al. 2006). The reflectivity-based parameter was maximum expected size of hail (MESH; Witt et al. 1998a; Lakshmanan et al. 2007). The two velocity-based parameters examined were the maximum storm-top divergent outflow (STD; Witt and Nelson 1991) and maximum mid-altitude rotational velocity (MRV; Witt 1998)[1]. The STD and MRV were calculated as:

$$STD = V_{max} - V_{min} \tag{1}$$

$$MRV = (V_{max} - V_{min})/2 \tag{2}$$

where V_{min} and V_{max} are the peak inbound and outbound velocities in the storm's divergence and rotation signatures. To minimize errors in the measurement of STD and MRV, only radial velocity data with corresponding reflectivity $\geq$ 15 dBZ and spectrum width $<$ 13 m s^{-1} were used. An additional criterion, to avoid use of unreliable data, was that a candidate velocity have sufficient spatial continuity with neighboring velocities on the same elevation scan, defined here as at least one adjacent velocity value within 5 m s^{-1} of the candidate velocity value.

The dual-polarization observations from KOUN, KCRI and KTLX on the lowest elevation scan (0.5°) associated

*Corresponding author address: Arthur Witt, NOAA/National Severe Storms Laboratory, 120 David L. Boren Blvd., Norman, OK, 73072.
E-mail: Arthur.Witt@noaa.gov

[1]For this study, mid-altitude was 3–9 km above radar level (ARL).

with the hail reports were examined as the storms passed over the location of each report. This included analysis of reflectivity (Z), differential reflectivity (Z_{DR}), copolar correlation coefficient (ρ_{HV}) and specific differential phase (K_{DP}) (see Kumjian 2013, for a description of the polarimetric radar variables). Measures of these variables were calculated using the median value of the eight radar bins within a 1° x 1 km window centered on the location of the hail report for the 0.5° elevation scan closest in time to the report time. If the original report time appeared to be in error [as is frequently the case: Witt et al. (1998b); Blair et al. (2017)], a corrected report time, estimated from radar data, was used instead.

Also examined for the AH was Z_{DR} column size. Z_{DR} column size was calculated by summing the number of 0.0025° x 0.0025° latitude-longitude grids output by the Z_{DR} column depth algorithm (Snyder et al. 2015) that had a depth $\geq$ 1 km for each volume scan. Z_{DR} column size is therefore an approximation of size based on the number of grids reaching this 1 km threshold.

3. RADAR SCANNING STRATEGIES

For the time period analyzed in this study, KOUN was operated manually using 90° sector scans and two volume coverage patterns (VCPs) specially designed to optimize spatial and temporal resolution (Table 3). From 2100–2114 and 2200–2343, KOUN used VCP-1; otherwise, VCP-2 was used. KCRI used a newly developed general-surveillance strategy (VCP-215) combined with one supplemental 0.5° intra-volume elevation scan (referred to as SAILS = Supplemental Adaptive Intra-Volume Low-Level Scan). KTLX used the operational severe-weather-surveillance strategy VCP-212 combined with two SAILS.

4. RADAR OBSERVATIONS

a. Character and evolution of storm intensity for the Paoli hailstorm

At 2100, the PH was still in the early stages of its development, having a maximum Z of 35 dBZ. Over the next 30 min, the PH steadily strengthened, with MESH increasing from 1 mm at 2106 (the first non-zero MESH) to 23 mm at 2127 (Fig. 2). MESH remained ~20 mm until 2205, afterwhich it rapidly increased to a peak of 45 mm at 2225. Unfortunately, from 2226–2306, it was not possible to accurately calculate MESH for the PH from KOUN, due to $Z > 40$ dBZ (the minimum Z used to calculate MESH) extending above the top elevation scan being used by KOUN during this time period. However, the MESH from KCRI (which is nearly co-located with KOUN) shows that the PH weakened very rapidly after 2225. It then quickly strengthened again, with MESH (from KCRI) reaching a secondary peak of 41 mm at 2255. From 2255 to 2337, the PH oscillated in strength, with MESH fluctuating rapidly within a range of ~20–40 mm. This was then followed by a more sustained weakening phase until 0007, afterwhich a final increase in stength occurred, with MESH reaching a final cyclical peak at 0021.

The STD and MRV followed a similar pattern to MESH, although the maximum STD and MRV occurred somewhat later (at 2241 and 2249, respectively) than MESH (Figs. 3, 4). Note that STD is not shown for KOUN because it did not scan the upper regions of the PH after 2136 (i.e., during the period of strongest storm intensity). The maximums in storm intensity as seen by MESH (at 2225), STD (at 2241) and MRV (at 2249) correspond closely in time with the maximum reported hail size (64 mm at 2240) for the PH, although the maximum predicted size of 45 mm is somewhat lower than the observed maximum size.

b. Character and evolution of storm intensity for the Ada hailstorm

The AH occurred farther southeast than the PH, allowing all three radars to fully scan the storm. The AH initially strengthened more slowly than the PH, with a first peak in MESH ~15 mm at 2158 (Fig. 5). The storm then weakened to the point that MESH decreased to near zero at 2219. Following this minimum, the storm underwent a more substantial period of strengthening, with MESH reaching 43 mm at 2307. A major, but short-lived, decrease in MESH then occurred, afterwhich new storm-cell development on the southwest flank of the storm resulted in another strengthening phase, lasting until 2333. Another weakening phase (in MESH) ensued, ending at 2246. Once again, new storm-cell development on the southern flank of the storm led to a major and rapid increase in strength, with MESH ultimately reaching a maximum of 64 mm (from KOUN) at 0020.

From 2145–2301, the STD followed a similar pattern to MESH, afterwhich the STD decreased only modestly (until ~2246) compared to the highly cyclical pattern in MESH ((Fig. 6). The STD then generally increased, reaching a maximum of 90 m s^{-1} at 0047. Significant mid-altitude rotation did not develop in the AH until ~2240, afterwhich it increased substantially to an initial peak of 28 m s^{-1} at 2320. Following this initial peak in MRV, it remained fairly steady in a range between ~20–30 m s^{-1}, ultimately reaching a maximum of 32 m s^{-1} at 0037. As with the PH, the maximums in storm intensity as seen by MESH (at 0020), STD (at 0047) and MRV (at 0037) correspond closely in time with the maximum reported hail size (83 mm at 0032). However, once again, the maximum predicted size of 64 mm is somewhat lower than the observed maximum size.

An analysis of Z_{DR} column depth size relative to MESH revealed that peaks in Z_{DR} column depth size probably preceded peaks in MESH (Fig. 7). This finding is consistent with other ongoing work that noted peaks in Z_{DR}

column depth size about 12 min prior to peaks in $-20°$C reflectivity core size (Kuster et al. 2017). In this case, the first relative peak (i.e., maximum) in Z_{DR} column depth size occurred at about 2246. After this time, two peaks in MESH occurred at about 2249 and 2307 (3–21 min after the peak in Z_{DR} column depth size). We observed the next relative peak in Z_{DR} column depth size at about 2325, which was about 5 min prior to the next relative peak in MESH at 2330. The final peak in Z_{DR} column depth size was reached at 2339 whereas MESH reached its final peak at about 0021 (Fig. 5). An analysis of Z_{DR} column depth size was not performed after 2342 due to hail contamination. Z_{DR} column depth size peaking prior to peaks in MESH could be important because the first peak in Z_{DR} column depth size occurred 8 and 20 min prior to severe hail reports, whereas the peaks in MESH occurred only a few minutes before or at about the same time as the hail reports in this case (Fig. 7).

c. Low-altitude dual-polarization observations

The overall character of the dual-polarization observations from KOUN, KCRI and KTLX on the 0.5° elevation scan associated with the hail reports were similar for Z, ρ_{HV} and K_{DP} for all three radars (Fig. 8). However, for Z_{DR}, KOUN had notably lower values ($\sim$1 dB lower) compared to KCRI and KTLX. Around half of this difference is due to a system bias of -0.5 dB in the KOUN Z_{DR} values. A slightly shorter wavelength for KOUN versus KCRI and KTLX (shorter for KOUN) might account for some of remaining Z_{DR} difference, due to higher attenuation in the hail cores.

5. CONCLUSIONS

For the two hailstorms analyzed in this study, the patterns of MESH, STD and MRV were well matched for the three radars, although KOUN tended to have higher relative maximum values at cyclical peaks of intensity, likely due to better temporal and spatial sampling. However, given the rapid changes in storm intensity seen multiple times for both hailstorms, the shorter volume update times from KOUN provided a better representation of storm intensity via multiple observations around peaks, toughs and periods of large increase or decrease in parameter magnitudes. For both hailstorms, maximums in MESH occurred 10–20 min prior to the largest reported hail size, with maximums in STD and MRV observed within 20 min. Based on this work and other ongoing work with rapid-scan KOUN data (Kuster et al. 2017), cyclical maximums in Z_{DR} column size may occur prior to cyclical maximums in upper-level reflectivity core magnitude and MESH. The low-altitude dual-polarization observations associated with the hail reports from the two storms show similar ranges of Z, ρ_{HV} and K_{DP} for the three radars, but notably lower Z_{DR} for KOUN vs KCRI and KTLX, with half of this difference due to a system bias of -0.5 dB in the KOUN Z_{DR} values.

References

Blair, S. F., and Coauthors, 2017: High-resolution hail observations: Implications for nws warning operations. *Weather and Forecasting*, **32 (3)**, 1101–1119, doi:10.1175/WAF-D-16-0203.1.

Kumjian, M. R., 2013: Principles and applications of dual-polarization weather radar. Part I: Description of the polarimetric radar variables. *J. Operational Meteor.*, **1 (19)**, 226–242, doi:10.15191/nwajom.2013.0119.

Kuster, C. M., J. C. Snyder, P. L. Heinselman, and T. J. Schuur, 2017: Rapid-scan dual-polarization radar observations of Z_{DR} column depth in the context of forecaster conceptual models. *Extended Abstracts, 38th Conf. on Radar Meteorology*, Chicago, IL, Amer. Meteor. Soc., 19A.5, [Available online at https://ams.confex.com/ams/38RADAR/meetingapp.cgi/Paper/320591.].

Lakshmanan, V., T. Smith, K. Hondl, G. J. Stumpf, and A. Witt, 2006: A real-time, three-dimensional, rapidly updating, heterogeneous radar merger technique for reflectivity, velocity, and derived products. *Wea. Forecasting.*, **21**, 802–823, doi:10.1175/WAF942.1.

Lakshmanan, V., T. Smith, G. Stumpf, and K. Hondl, 2007: The Warning Decision Support System – Integrated Information. *Wea. Forecasting.*, **22**, 596–612, doi:10.1175/WAF1009.1.

Snyder, J. C., A. V. Ryzhkov, M. R. Kumjian, A. P. Khain, and J. Picca, 2015: A Z_{DR} column detection algorithm to examine convective storm updrafts. *Weather and Forecasting*, **30 (6)**, 1819–1844, doi:10.1175/WAF-D-15-0068.1.

Witt, A., 1998: The relationship between WSR-88D measured midaltitude rotation and maximum hail size. Preprints, *19th Conference on Severe Local Storms*, Minneapolis, MN, Amer. Meteor. Soc., 740–743.

Witt, A., M. D. Eilts, G. J. Stumpf, J. T. Johnson, E. D. W. Mitchell, and K. W. Thomas, 1998a: An enhanced hail detection algorithm for the WSR-88D. *Wea. Forecasting.*, **13**, 286–303, doi:10.1175/1520-0434(1998)013⟨0286:AEHDAF⟩2.0.CO;2.

Witt, A., M. D. Eilts, G. J. Stumpf, E. D. W. Mitchell, J. T. Johnson, and K. W. Thomas, 1998b: Evaluating the performance of WSR-88D severe storm detection algorithms. *Wea. Forecasting.*, **13**, 513–518, doi:10.1175/1520-0434(1998)013⟨0513:ETPOWS⟩2.0.CO;2.

Witt, A., and S. P. Nelson, 1991: The use of single-Doppler radar for estimating maximum hailstone size. *J. Appl. Meteor.*, **30**, 425–431, doi:10.1175/1520-0450(1991)030⟨0425:TUOSDR⟩2.0.CO;2.

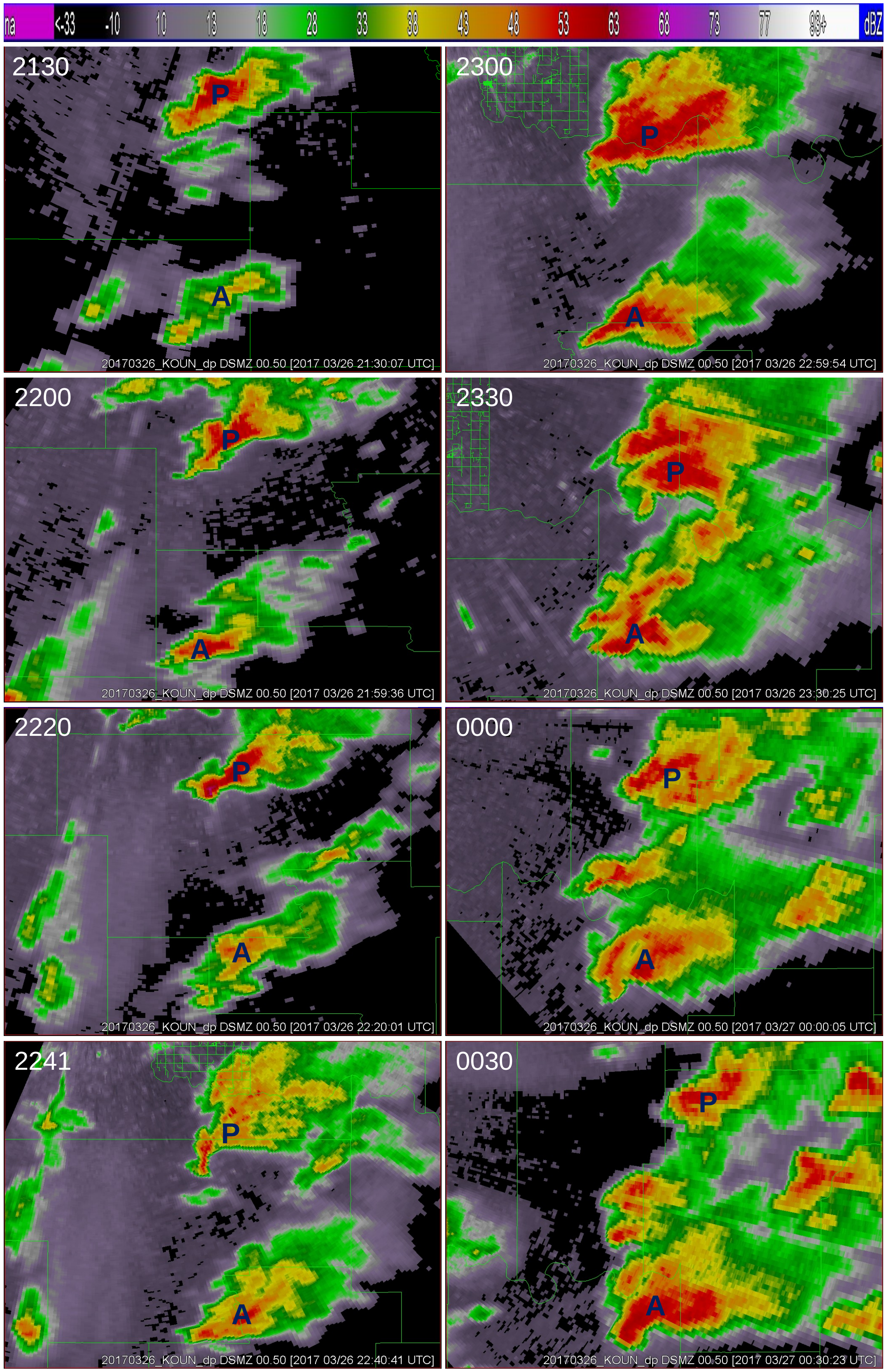

FIG. 1. KOUN reflectivity from the 0.5° elevation scan for the Paoli (P) and Ada (A) hailstorms at 20–30 min intervals, with the image time in the top-left corner.

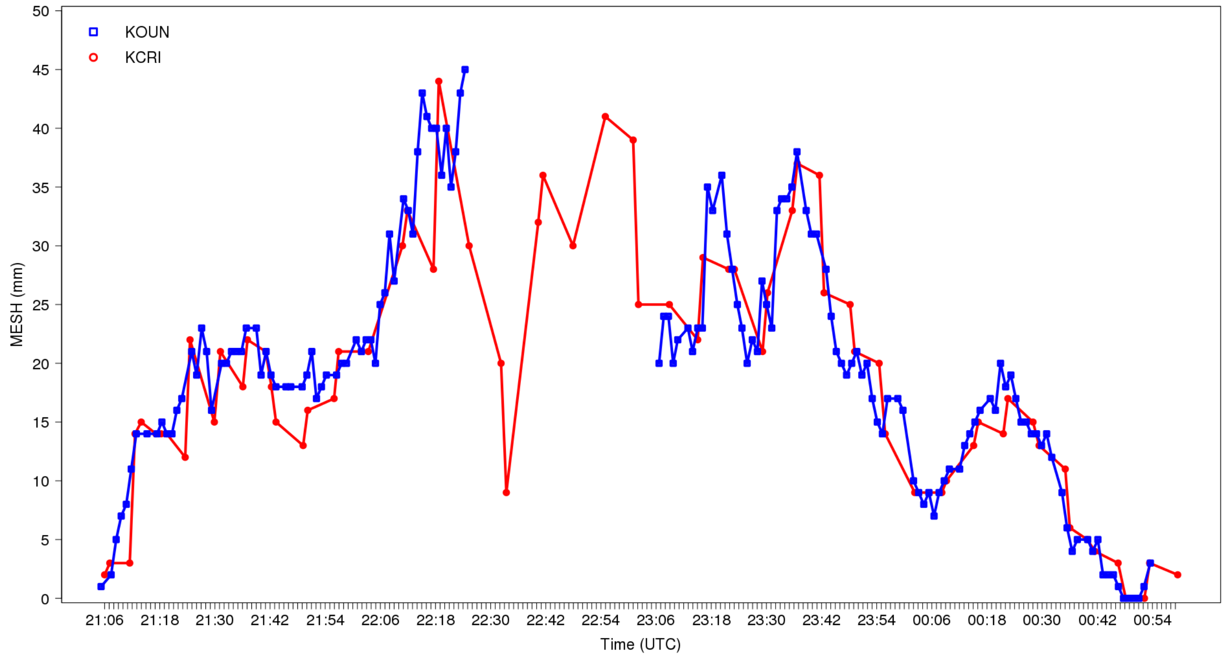

FIG. 2. MESH derived from KOUN and KCRI for the Paoli hailstorm. For display clarity, the seconds component of the times shown on the bottom axis, for this and other time/value plots, have been truncated.

FIG. 3. STD derived from KCRI and KTLX for the Paoli hailstorm.

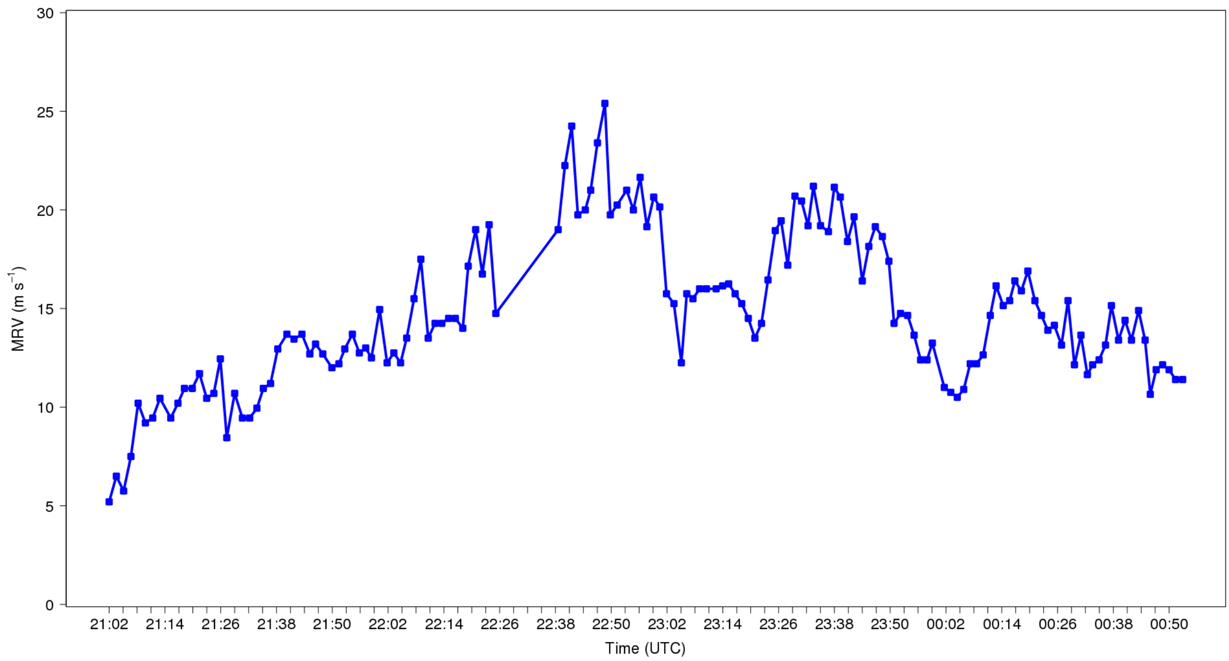

FIG. 4. MRV derived from KOUN for the Paoli hailstorm.

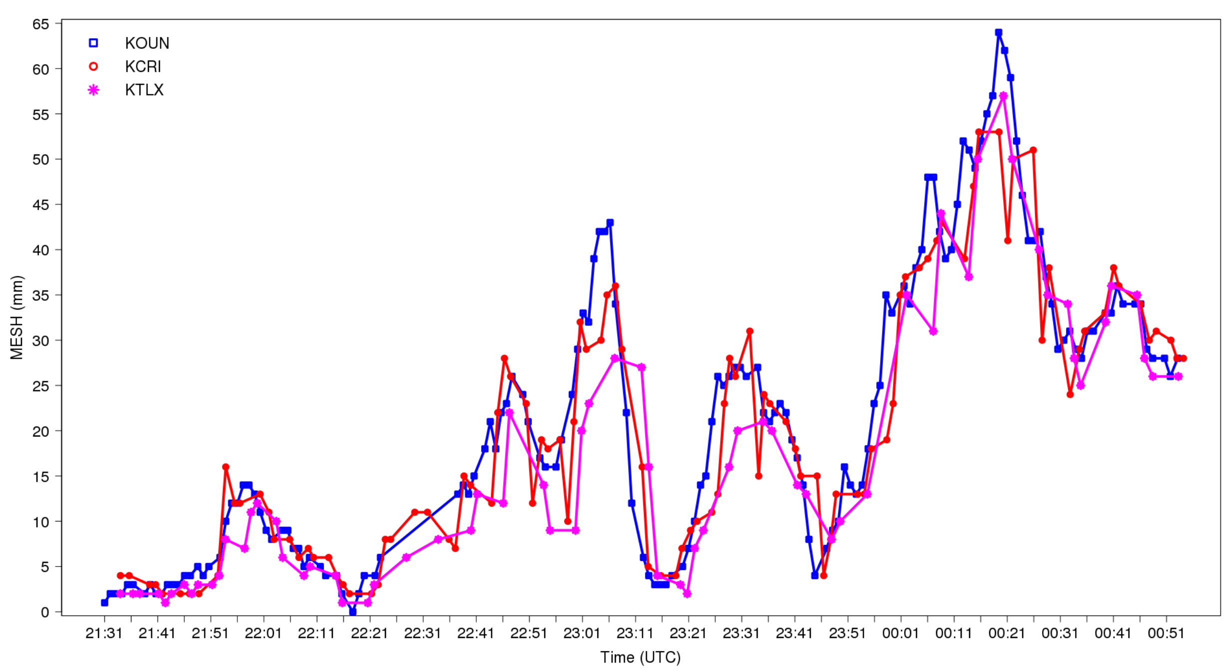

FIG. 5. MESH derived from KOUN, KCRI and KTLX for the Ada hailstorm.

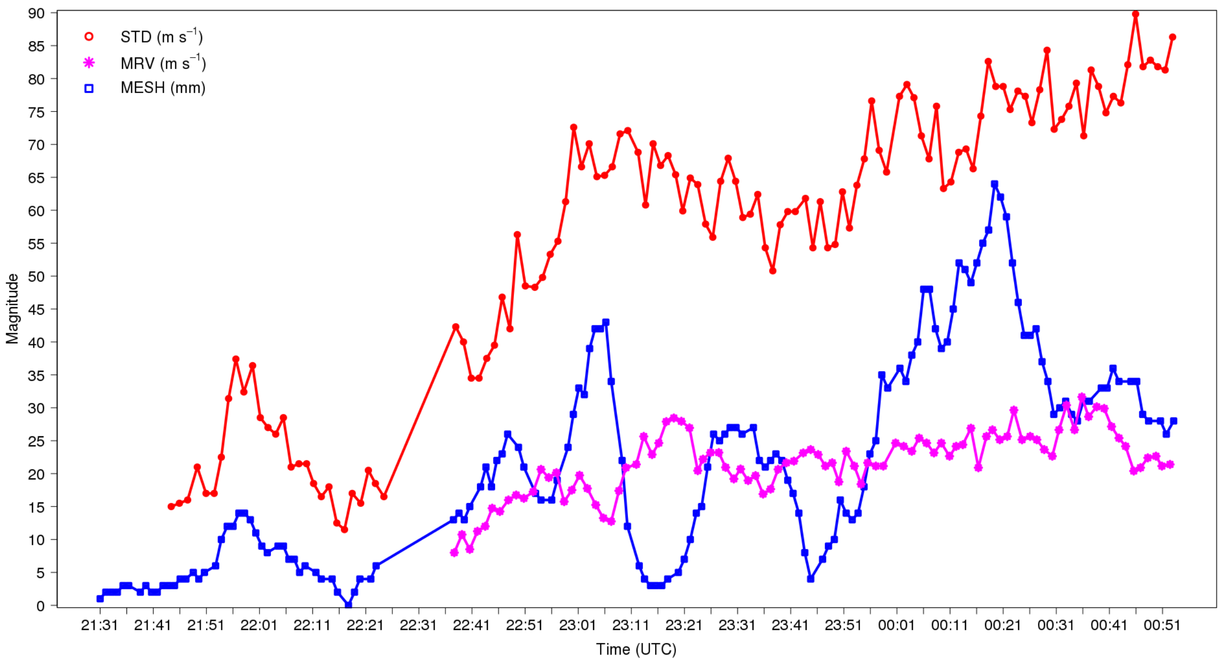

FIG. 6. STD, MRV and MESH derived from KOUN for the Ada hailstorm.

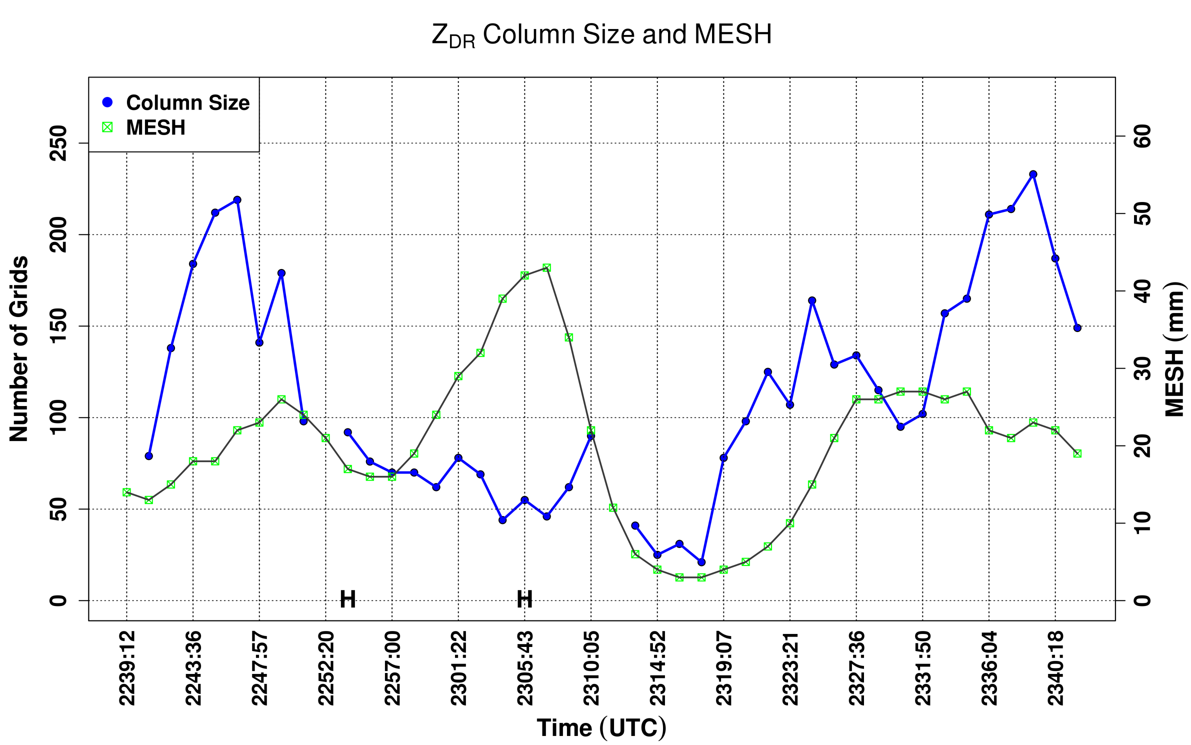

FIG. 7. Z_{DR} column depth size (blue line) and MESH (black line with green markers) derived from KOUN for the Ada hailstorm. H indicates the time of a severe hail report.

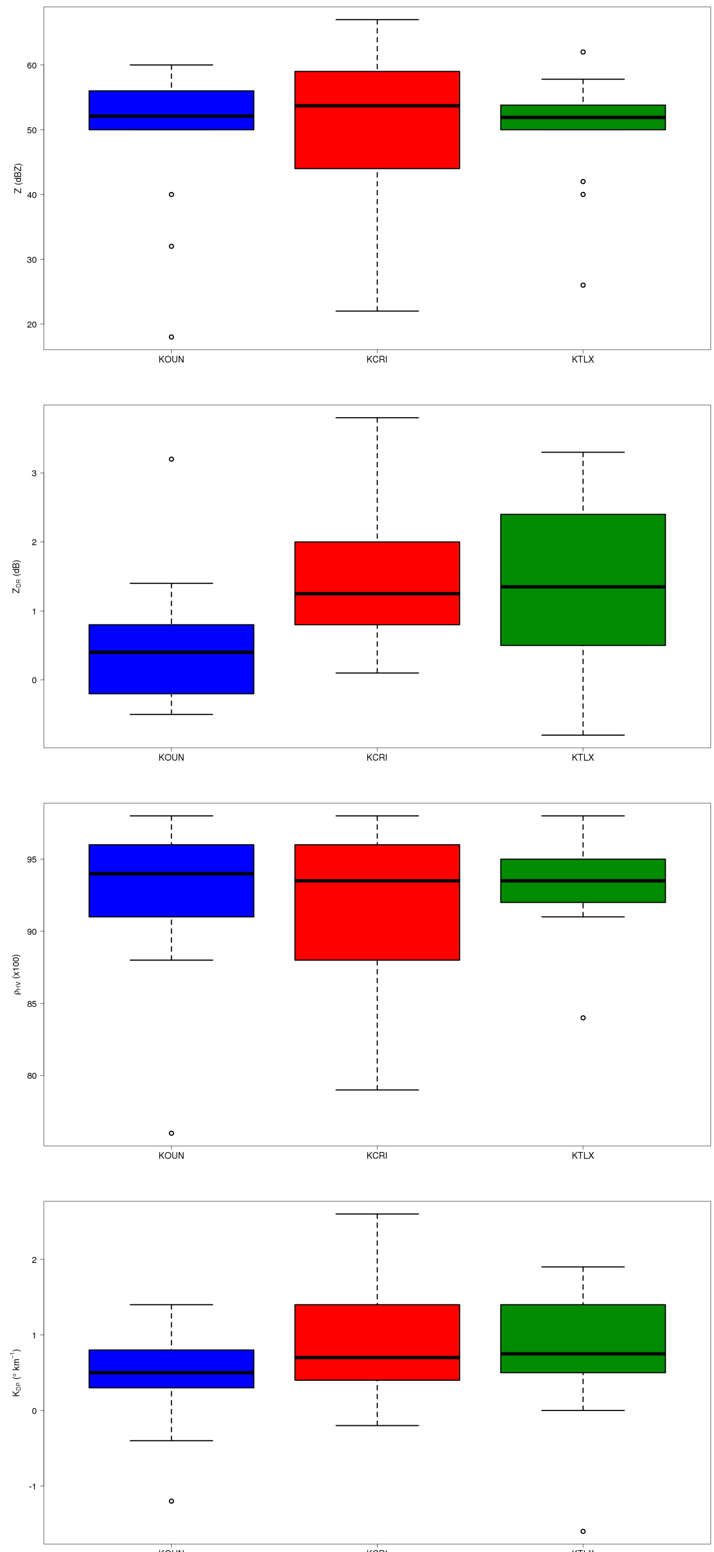

FIG. 8. Box plots of reflectivity (Z), differential reflectivity (Z_{DR}), co-polar correlation coefficient (ρ_{HV}) and specific differential phase (K_{DP}) from the 0.5°elevation scans of KOUN, KCRI and KTLX associated with the hail reports.

TABLE 1. List of the hailstone reports from the Paoli hailstorm.

Time (UTC)	Latitude (°)	Longitude (°)	Size (mm)
2155	34.67	−97.42	25
2239	34.80	−97.25	44
2240	34.83	−97.24	64
2250	34.86	−97.11	38
2250	34.83	−97.17	44
2255	34.83	−97.10	44
2351	35.11	−96.68	25

TABLE 2. List of the hailstone reports from the Ada hailstorm.

Time (UTC)	Latitude (°)	Longitude (°)	Size (mm)
2254	34.60	−97.03	57
2306	34.64	−97.09	38
2354	34.78	−96.68	25
0001	34.74	−96.64	28
0008	34.76	−96.68	44
0032	34.80	−96.51	83
0043	34.86	−96.41	44
0050	34.81	−96.41	47

TABLE 3. Radar scanning strategies. VCP = Volume Coverage Pattern, and SAILS = Supplemental Adaptive Intra-Volume Low-Level Scan.

Radar	VCP Elevation Angles (°)	Update Time (min)
KOUN	VCP-1: 0.5, 0.9, 1.4, 2.4, 3.5, 4.6, 5.7, 7.1, 9.1, 11.4	1.5
KOUN	VCP-2: 0.5, 0.9, 1.4, 2.0, 2.7, 3.5, 4.4, 5.5, 6.5, 7.7	1.4
KCRI	VCP-215 + 1 SAILS: 0.5, 0.9, 1.3, 1.8, 2.4, 3.1, 0.5, 4.0, 5.1, 6.4, 8.0, 10.0, 12.0, 14.0, 16.7, 19.5	7.1
KTLX	VCP-212 + 2 SAILS: 0.5, 0.9, 1.3, 0.5, 1.8, 2.4, 3.1, 4.0, 5.1, 0.5, 6.4, 8.0, 10.0, 12.5, 15.6, 19.5	6.0